PACS numbers: 05.10.Ln, **64.60.–i**, **75.40.–s**
DOI: 10.1070/PU2008v051n09ABEH006611

Critical properties of frustrated spin systems on a stacked triangular lattice

A K Murtazaev

1. Introduction

One of the fundamental problems in statistical physics is the study of phase transitions and critical phenomena in frustrated spin systems. Despite the achievements in this area of research, the question of building a rigorous and consistent microscopic theory remains central to the modern condensed matter physics [1]. The modern theory of phase transitions and critical phenomena is based mainly on the ideas put forward in the hypothesis of scaling and universality and in the renormalization group theory [1–4]. Analysis of the results obtained from studies of frustrated systems and spin systems with quenched nonmagnetic disorder has shown that many of these results go far beyond the modern theory of phase transitions and critical phenomena [3, 5, 6].

Most of the traditional theoretic and experimental studies of frustrated systems encounter serious difficulties in attempts to calculate the critical parameters and to determine the features, nature, and mechanisms of critical behavior [7, 8]. Therefore, phase transitions and critical phenomena are currently studied by Monte Carlo methods [7–13]. Only lately did the study of the immediate vicinity of the critical point by Monte Carlo methods become possible. The achievements in this field are not only due to the sharp increase in computing power but also a result of new ideas and methods being developed. In particular, special algorithms, known as replica algorithms, for Monte Carlo calculations have been developed to study frustrated systems.

Currently, the magnetic, thermal, and critical properties of frustrated spin systems are being carefully studied [12, 13, 15–20], and the reason is that frustrated systems have remarkable magnetic properties and a rich variety of phases and phase transitions caused by strong degeneracy and a high susceptibility of such systems to various perturbing interactions [21, 22]. Moreover, it is still unclear whether frustrated spin systems belong to a new universality class of critical behavior and its dependence on various factors, such as the type and magnitude of the interlayer exchange coupling, the next-nearest-neighbor interaction, anisotropy, and external magnetic field.

In this report, we consider the results of a Monte Carlo investigation of the critical properties of the model of a 3D Heisenberg antiferromagnet on a triangular lattice.

The interest in this model stems from the fact that antiferromagnets on a triangular lattice constitute an example of frustrated systems. By studying this model, we may hope to resolve the question of whether frustrated systems belong to a new universality class of critical behavior, which is still open for discussion [6–13]. Furthermore, many important physical properties of frustrated systems strongly depend on the lattice geometry (on the degree of frustration). These features may narrow the possible universality classes of critical behavior, but there is still much to be done in this respect.

The question of the dependence of the critical properties of frustrated systems on the magnitude of the interlayer exchange coupling is especially interesting. The critical exponents, which are highly sensitive parameters, may serve as indicators of the spatial crossover from the 3D critical behavior to the 2D one (and back). The data that are currently at our disposal are not sufficient to uniquely determine how the critical behavior of frustrated systems depends on the interlayer exchange coupling parameter, and the problem has yet to be solved [8, 9, 12, 13].

In addition, the dependence of the critical properties of frustrated systems on the type and magnitude of the interlayer exchange coupling is not described in the available literature.

In this review, within a single method, and using a reliable scheme based on a special algorithm for the Monte Carlo methods (the replica algorithm), we attempt to determine the values of the critical parameters of models of frustrated 3D Heisenberg antiferromagnets on a triangular lattice with the highest possible accuracy.

2. The model and the method

The Hamiltonian of a 3D Heisenberg antiferromagnet on a triangular lattice can be written as [3]

$$\mathrm{H} = -J\sum_{\langle ij\rangle}\mathbf{S}_i\mathbf{S}_j - J'\sum_{\langle ij\rangle}\mathbf{S}_i\mathbf{S}_j\,, \tag{1}$$

where $\mathbf{S}_i = (S_i^x, S_i^y, S_i^z)$ is a three-component unit vector, and J and J' are the exchange coupling constants. Summation is over the nearest neighbors. The lattice consists of 2D triangular layers packed along the orthogonal axis. The first term in the right-hand side of Eqn (1) accounts for the intralayer exchange coupling J and the second term accounts for the interlayer coupling J'.

We use three models, called D_1, D_2, and D_3, to establish the effect of the type and magnitude of the interlayer exchange coupling on the nature of the critical behavior:

model D_1: $J<0,\ J'>0,\ |J|=|J'|$;
model D_2: $J<0,\ J'<0,\ |J|=|J'|$;
model D_3: $J<0,\ J'>0,\ |J|\neq|J'|$.

Frustrated spin systems are complicated objects, even for studies by Monte Carlo methods. As is known, near a critical point, Monte Carlo methods encounter what is known as the critical-slowing-down problem; this problem is even more acute with frustrated systems [7]. Moreover, a characteristic feature of frustrated systems is the problem of multiple valleys of local energy minima. Ordinary Monte Carlo methods are usually ill suited for solving this problem. Hence, many new variants of these methods have recently been developed that focus on studies of frustrated systems. Among these, the replica algorithms have proved to be the most powerful and effective in the studies of critical phenomena in frustrated systems [14].

In our investigation, we used the highly effective replica algorithm [14] of the following type:

(i) Two replicas X and X' with different temperatures T and T' are modeled simultaneously.

(ii) After one hundred Monte Carlo steps per spin have been completed, the replicas exchange data in accordance with the Metropolis scheme with the probability

$$w(X\to X') = \begin{cases} 1\,, & \Delta\leqslant 0\,,\\ \exp(-\Delta)\,, & \Delta>0\,, \end{cases}$$

where $\Delta = (T - T')(U - U')$, with U and U' being the respective internal energies of the first and second replicas.

In the replica exchange algorithm, a random walk along the 'temperature interval' is implemented for each replica, with each random walk stimulating a random walk in the potential energy field. This facilitates the solution of the problem of the system 'sticking' in many states with local energy minima.

The calculations were carried out for systems with periodic boundary conditions and with linear dimensions $L \times L \times L = N$, where $L = 9-30$ for the D_1 and D_3 models and $L = 12-42$ for the D_2 model. For the D_3 model, the ratio of the interlayer to intralayer exchanges varied in the interval $R = |J'/J| = 0.01-1.0$. To take the system out of the state of thermodynamic equilibrium, a section of $\tau_0 = 4.0 \times 10^5$ Monte Carlo steps per spin, which is several times longer than the nonequilibrium section, was cut out. The thermodynamic quantities were averaged along a Markov chain $\tau = 25\tau_0$ long. To increase the accuracy, the data obtained from ten different initial configurations were averaged.

3. Simulation results

To monitor the temperature behavior of the heat capacity and susceptibility, we used the expressions [1, 23–25]

$$C = NK^2\left(\langle U^2\rangle - \langle U\rangle^2\right), \tag{2}$$

$$\chi = \begin{cases} NK\left(\langle m^2\rangle - \langle m\rangle^2\right), & T < T_{\mathrm{N}}, \\ NK\langle m^2\rangle, & T \geqslant T_{\mathrm{N}}, \end{cases} \tag{3}$$

$$\chi_{\mathrm{ch}} = \begin{cases} NK\left(\langle m_{\mathrm{ch}}^2\rangle - \langle m_{\mathrm{ch}}\rangle^2\right), & T < T_{\mathrm{ch}}, \\ NK\langle m_{\mathrm{ch}}^2\rangle, & T \geqslant T_{\mathrm{ch}}, \end{cases} \tag{4}$$

where $K = |J|/k_{\mathrm{B}}T$, N is the number of particles, m is the magnetic order parameter, m_{ch} is the chiral order parameter, and χ_{ch} is the chiral susceptibility.

The order parameter m of the system is given by [9]

$$m = \frac{3}{N}\sqrt{\frac{\langle M_{\mathrm{A}}^2 + M_{\mathrm{B}}^2 + M_{\mathrm{C}}^2\rangle}{3}}, \tag{5}$$

where M_{A}, M_{B}, and M_{C} are the magnetization of the sublattices A, B, and C.

The magnetization of a sublattice is given by [9]

$$\left\langle |\mathbf{M}_r| \right\rangle = \left\langle \sqrt{S_x^2 + S_y^2 + S_z^2} \right\rangle, \qquad r = \mathrm{A}, \mathrm{B}, \mathrm{C}. \tag{6}$$

To calculate the chiral order parameter m_{ch} of the system, we use the expressions [10, 11]

$$m_{\mathrm{ch}p} = \frac{2}{3\sqrt{3}}\sum_{\langle ij\rangle}^{p}[\mathbf{S}_i \times \mathbf{S}_j]_z, \tag{7}$$

$$m_{\mathrm{ch}} = \frac{1}{N}\sum_{p} m_{\mathrm{ch}p}, \tag{8}$$

where the subscript p labels the triangular plaquettes.

Figures 1 and 2 show the temperature dependence of the heat capacity C and the susceptibility χ for models D_1 and D_2. Here and in what follows, the errors in the data do not exceed the size of the symbols in the figures. We note the distinct maxima in the critical region for both models, with the maxima occurring at the same temperature (within error).

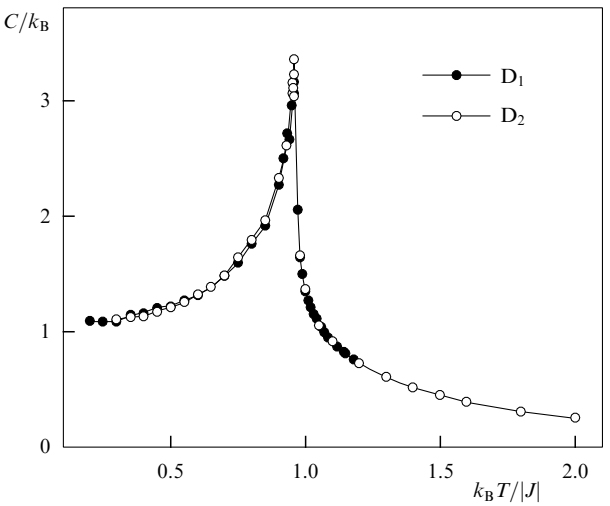

Figure 1. The heat capacity C/k_{B} as a function of the temperature $k_{\mathrm{B}}T/|J|$ for models D_1 and D_2.

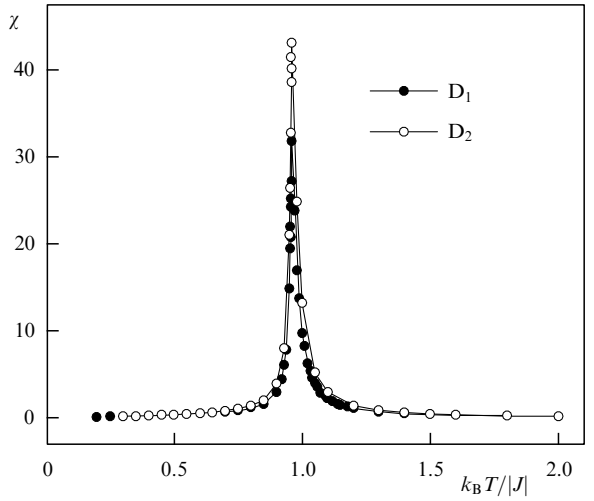

Figure 2. The susceptibility χ as a function of the temperature $k_{\mathrm{B}}T/|J|$ for models D_1 and D_2.

To determine the critical temperature T_{N} more accurately, we use the method of fourth-order Binder cumulants U_L, which are [26]

$$U_L = 1 - \frac{\langle m^4\rangle_L}{3\langle m^2\rangle_L^2}. \tag{9}$$

According to the finite-size scaling theory, the critical point is the point where all the temperature curves $U_L(T)$ intersect [25].

Figure 3 depicts the characteristic temperature dependence of U_L for model D_2. The inset shows the accuracy with which the critical temperature was determined. Clearly, the critical temperature at $R = 1$ is $T_{\mathrm{N}} = 0.957(1)$ (here and in what follows, the temperature is given in units of $|J|/k_{\mathrm{B}}$). In determining the chiral critical temperature T_{ch}, we used the cumulant crossing method, which is considered more accurate and reliable [11–13, 26, 27]. Similar calculations were done for models D_1 and D_3.

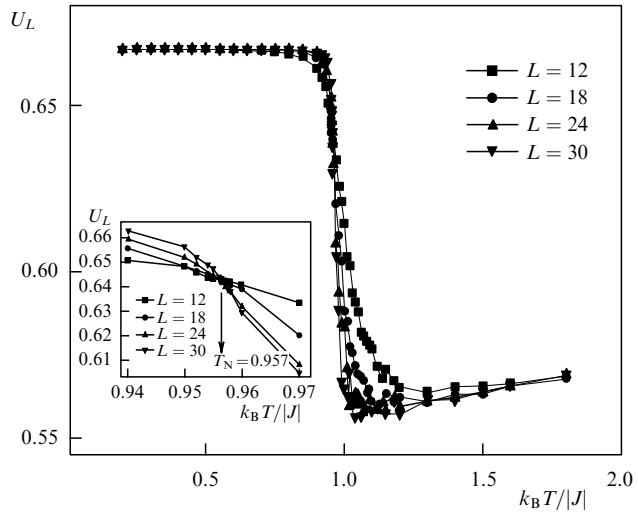

Figure 3. The Binder cumulant U_L as a function of the temperature $k_BT/|J|$ for model D_2.

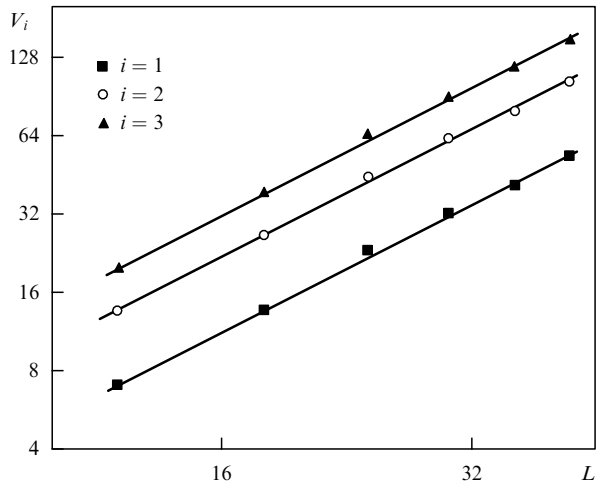

Figure 4. Dependence of the parameter V_i on the linear size L at $T = T_N$ for model D_2.

To calculate the static chiral and magnetic critical exponents of the heat capacity (α), of the susceptibilities (γ and γ_{ch}), of the magnetizations (β and β_{ch}), and of the correlation radii (ν and ν_{ch}), we used formulas from the finite-size scaling theory [24, 26–29].

It follows from the KPC relations that the following relations hold in a system with the dimensions $L \times L \times L$ at $T = T_N$ for sufficiently large L [11, 24, 28–31]:

$$m \propto L^{-\beta/\nu}, \tag{10}$$

$$m_{ch} \propto L^{-\beta_{ch}/\nu_{ch}}, \tag{11}$$

$$\chi \propto L^{\gamma/\nu}, \tag{12}$$

$$\chi_{ch} \propto L^{\gamma_{ch}/\nu_{ch}}, \tag{13}$$

$$V_n = L^{1/\nu} g_{V_n}, \tag{14}$$

$$V_{chn} = L^{1/\nu_{ch}} g_{V_n}, \tag{15}$$

where g_{V_n} is a constant and V_n and V_{chn} can be taken as

$$V_i = \frac{\langle m^i E\rangle}{\langle m^i\rangle} - \langle E\rangle, \qquad i = 1,2,3,4, \tag{16}$$

$$V_{chi} = \frac{\langle m_{ch}^i E\rangle}{\langle m_{ch}^i\rangle} - \langle E\rangle, \qquad i = 1,2,3,4. \tag{17}$$

These relations were used to determine β, β_{ch}, γ, γ_{ch}, ν, and ν_{ch}. In approximating the temperature dependence of the heat capacity on L, we used the expression [9–11, 32]

$$C_{max}(L) = A_1 - A_2 L^{\alpha/\nu}, \tag{18}$$

where A_1 and A_2 are some coefficients.

Figure 4 shows the characteristic curves representing the dependence of the parameters V_i for $i = 1, 2, 3$ on the lattice size L for model D_2 in the log-log scale. Clearly, points in the diagrams land on straight lines (within error). The diagrams in Fig. 4 obtained by the method of least squares are parallel straight lines, and their slopes determine the value of $1/\nu$. The value of ν calculated in this manner was used to determine the critical exponents of the heat capacity (α), susceptibility (γ), and magnetization (β). The chiral critical exponents were also determined through this scheme. Similar calculations were carried out for models D_1 and D_3.

All the values of the exponents thus obtained are listed in Table 1. The data in Refs [6, 7, 9–11] are also listed for comparison.

Of special interest is the procedure that was used to determine the Fisher exponent η. Starting from the relation between the susceptibility χ and the correlation radius ξ [33],

$$\chi \propto \xi^{\gamma/\nu}, \tag{19}$$

and using the relation $\eta = 2 - \gamma/\nu$ between the exponents η and ν, we obtain

$$\ln \frac{\chi}{\xi^2} = c - \eta \ln \xi, \tag{20}$$

where c is a constant. For a finite-size system at $T = T_N$, we have $\xi = L$. This yields

$$\ln \frac{\chi}{L^2} = c - \eta \ln L. \tag{21}$$

Using this formula, we determined the Fisher exponent η. The same approach was used to determine the magnetic and chiral critical Fisher exponents for models D_1 and D_2, which are also listed in Table 1.

The values of the magnetic and chiral critical temperatures for models D_1 and D_2 coincide, to within error, with each other and with those obtained in [9–11]. A comparison of the values of the critical exponents for model D_1 and the results for a similar model in [9, 11] shows that our data are close to those in the more recent paper [11]. Some of the critical parameters for model D_2 coincide, to within error, with the results for the same model in Ref. [10]. Table 1 shows that our data for model D_1 are closer to the experimental results (see the references in [6]) for the antiferromagnet $CsMnBr_3$ with a triangular lattice than to the data for model D_2. We note that this is the first time that the values of the Fisher exponents η and η_{ch} for models D_1 and D_2 have been calculated.

Table 1 clearly shows that our results are in good agreement with the data from laboratory experiments and

Table 1. Values of the critical parameters for a 3D Heisenberg antiferromagnet on a stacked triangular lattice.

Critical parameter	Our data		Monte Carlo method			Experiment (see references in [6])	Pure model (see references in [7])
	D_1	D_2	[9]	[10]	[11]		
T_N	0.956(1)	0.957(1)	0.954(2)	0.955(2)	0.9577(2)	—	1.443
T_{ch}	0.956(2)	0.957(2)	—	0.958(2)	0.9577(2)	—	—
ν	0.59(1)	0.64(1)	0.53(3)	0.59(2)	0.586(8)	0.57(3)	0.706(9)
α	0.26(2)	0.05(2)	0.4(1)	0.24(8)	—	0.40(5)	−0.117(2)
β	0.26(1)	0.30(1)	0.25(2)	0.30(2)	0.285(11)	0.25(1)	0.364(7)
γ	1.23(2)	1.36(2)	1.1(1)	1.17(7)	1.185(3)	1.10(5)	1.390(23)
ν_{ch}	0.59(2)	0.64(2)	—	0.60(2)	0.60(2)	—	—
β_{ch}	0.43(2)	0.52(2)	—	0.55(2)	0.50(2)	0.44(2)	—
γ_{ch}	0.87(3)	0.93(3)	—	0.72(2)	0.82(2)	0.84(7)	—
η	−0.09(3)	−0.06(3)	—	—	—	—	0.031(7)
η_{ch}	0.50(4)	0.63(4)	—	—	—	—	—

Table 2. Values of the magnetic critical parameters for model D_3.

R	T_N	ν	α	β	γ	$\alpha+2\beta+\gamma=2$
1	0.956(1)	0.59(2)	0.26(3)	0.26(2)	1.23(4)	2.02
0.8	0.872	0.60	0.24	0.26	1.26	2.02
0.7	0.829	0.61	0.22	0.28	1.29	2.07
0.6	0.783	0.59	0.22	0.29	1.22	2.02
0.4	0.677	0.60	0.24	0.27	1.27	2.05
0.3	0.619	0.60	0.26	0.29	1.23	2.07
0.1	0.468	0.59	0.24	0.28	1.17	1.97
0.075	0.442	0.55	0.26	0.24	1.23	1.97
0.05	0.413	0.55	0.15	0.22	1.11	1.70
0.01	0.353	0.48	0.09	0.27	0.82	1.45

Table 3. Values of the chiral critical parameters for model D_3.

R	T_{ch}	ν_{ch}	α	β_{ch}	γ_{ch}	$\alpha+2\beta_{ch}+\gamma_{ch}=2$
1	0.956(2)	0.59(2)	0.26(3)	0.43(2)	0.87(5)	1.99
0.8	0.872	0.60	0.24	0.42	0.96	2.04
0.7	0.829	0.61	0.22	0.48	0.96	2.14
0.6	0.783	0.59	0.22	0.46	0.85	1.99
0.4	0.677	0.60	0.24	0.43	0.90	2
0.3	0.619	0.60	0.26	0.48	0.81	2.03
0.1	0.468	0.59	0.24	0.47	0.82	2
0.075	0.442	0.55	0.26	0.42	0.87	1.97
0.05	0.413	0.55	0.15	0.31	0.60	1.37
0.01	0.353	0.48	0.09	0.40	0.52	1.41

with most results of numerical experiments by other researchers, but differ from the results for a nonfrustrated 3D Heisenberg antiferromagnet (see the references in [7]). This suggests that the 3D Heisenberg frustrated antiferromagnet on a stacked triangular lattice (model D_1) constitutes a new universality class of critical behavior.

Moreover, most of the critical exponents of model D_1 differ significantly from the critical exponents of model D_2. This suggests that the type of interlayer exchange coupling plays an important role in the formation of universality classes of such systems. It is obvious that models D_1 and D_2 belong to different universality classes and each has its own set of critical exponents.

The question of the dependence of the critical exponents on R is also of considerable interest. Furthermore, for the majority of real materials, the values of J and J' do not coincide [15–17, 20]. This question was studied for different values of R. Using a relation from the finite-size scaling theory and the above procedure, we were able to calculate all the main static chiral and magnetic critical exponents for $J<0$ and $J'>0$ with R ranging from 0.01 to 1.0. The values of the exponents obtained in this way are listed in Tables 2 and 3.

The data in Tables 2 and 3 show that for the values $R \geqslant 0.075$, the exponents coincide (within error) and scaling relations between the critical exponents hold with high accuracy. When $R \leqslant 0.05$, the critical exponents vary substantially and scaling relations are no longer valid. Apparently, $R = 0.075$ is the limit beyond which a crossover from the 3D critical behavior to the 2D critical behavior occurs.

4. Conclusion

The study of the critical properties of the 3D Heisenberg frustrated antiferromagnet on a stacked triangular lattice, whose results are presented in this report, has been done using the highly effective Monte Carlo replica algorithm. We have calculated the main static chiral and magnetic critical exponents. The critical exponents of heat capacity (α), susceptibilities (γ and γ_{ch}), order parameters (β and β_{ch}), Fisher exponents η and η_{ch}, and correlation radii (ν and ν_{ch}) were calculated using relations from the finite-size scaling theory within a single method and a single investigation. The values of the Fisher exponents η and η_{ch} for this model were calculated for the first time. Our results suggest that the 3D frustrated Heisenberg model antiferromagnet on a stacked triangular lattice belongs to a new universality class. The results of our investigation imply that the universality class of the critical behavior of the Heisenberg antiferromagnet on a triangular lattice depends on the type and magnitude of the interlayer exchange coupling.

This work was supported by the Russian Foundation for Basic Research (grant 07-02-00194 and the South Russia grant 06–02-96602) and the Russian Science Support Foundation.

References

1. Patashinskii A Z, Pokrovskii V L *Fluktuatsionnaya Teoriya Fazovykh Perekhodov* (Fluctuation Theory of Phase Transitions) 2nd ed. (Moscow: Nauka, 1982) [Translated into English (Oxford: Pergamon Press, 1979)]

2. Ma Sh *Modern Theory of Critical Phenomena* (Reading, Mass.: W.A. Benjamin, 1976) [Translated into Russian (Moscow: Mir, 1980)]
3. Dotsenko Vik S *Usp. Fiz. Nauk* **165** 481 (1995) [*Phys. Usp.* **38** 457 (1995)]
4. Korshunov S E *Usp. Fiz. Nauk* **176** 233 (2006) [*Phys. Usp.* **49** 225 (2006)]
5. Murtazaev A K *Usp. Fiz. Nauk* **176** 1119 (2006) [*Phys. Usp.* **49** 1092 (2006)]
6. Maleev S V *Usp. Fiz. Nauk* **172** 617 (2002) [*Phys. Usp.* **45** 569 (2002)]
7. Kamilov I K, Murtazaev A K, Aliev Kh K *Usp. Fiz. Nauk* **169** 773 (1999) [*Phys. Usp.* **42** 689 (1999)]
8. Loison D et al. *Pis'ma Zh. Eksp. Teor. Fiz.* **72** 487 (2000) [*JETP Lett.* **72** 337 (2000)]
9. Kawamura H *J. Phys. Soc. Jpn.* **56** 474 (1987)
10. Kawamura H *J. Phys. Soc. Jpn.* **61** 1299 (1992)
11. Mailhot A, Plumer M L, Caille A *Phys. Rev. B* **50** 6854 (1994)
12. Murtazaev A K, Ramazanov M K, Badiev M K *Zh. Eksp. Teor. Fiz.* **132** 1152 (2007) [*JETP* **105** 1011 (2007)]
13. Murtazaev A K, Ramazanov M K *Phys. Rev. B* **76** 174421 (2007)
14. Mitsutake A, Sugita Y, Okamoto Y *Biopolymers* **60** 96 (2001)
15. Svistov L E et al. *Phys. Rev. B* **67** 094434 (2003)
16. Svistov L E et al. *Pis'ma Zh. Eksp. Teor. Fiz.* **80** 231 (2004) [*JETP Lett.* **80** 204 (2004)]
17. Svistov L E et al. *Pis'ma Zh. Eksp. Teor. Fiz.* **81** 133 (2005) [*JETP Lett.* **81** 102 (2005)]
18. Pelissetto A, Rossi P, Vicari E *Phys. Rev. B* **65** 020403 (2001)
19. Peles A, Southern B W *Phys. Rev. B* **67** 184407 (2003)
20. Smirnov A I et al. *Phys. Rev. B* **75** 134412 (2007)
21. Gekht R S *Zh. Eksp. Teor. Fiz.* **102** 1968 (1992) [*JETP* **75** 1058 (1992)]
22. Gekht R S *Usp. Fiz. Nauk* **159** 2 (1989) [*Sov. Phys. Usp.* **32** 871 (1989)]
23. Binder K, Wang J-Sh *J. Stat. Phys.* **55** 87 (1989)
24. Peczak P, Ferrenberg A M, Landau D P *Phys. Rev. B* **43** 6087 (1991)
25. Binder K, Heermann D W *Monte Carlo Simulation in Statistical Physics* (Berlih: Springer-Verlag, 1988) [Translated into Russian (Moscow: Nauka, 1995)]
26. Binder K *Z. Phys. B* **43** 119 (1981)
27. Ferrenberg A M, Landau D P *Phys. Rev. B* **44** 5081 (1991)
28. Ferdinand A E, Fisher M E *Phys. Rev.* **185** 832 (1969)
29. Fisher M E, Barber M N *Phys. Rev. Lett.* **28** 1516 (1972)
30. Landau D P *Physica A* **205** 41 (1994)
31. Loison D *Phys. Lett. A* **257** 83 (1999)
32. Murtazaev A K, Kamilov I K, Magomedov M A *Zh. Eksp. Teor. Fiz.* **120** 1535 (2001) [*JETP* **93** 1330 (2001)]
33. Holm Ch, Janke W *Phys. Rev. B* **48** 936 (1993)

PACS numbers: **42.55.–f**, 42.60.By, **42.65.–k**
DOI: 10.1070/PU2008v051n09ABEH006612

Petawatt lasers based on optical parametric amplifiers: their state and prospects

E A Khazanov, A M Sergeev

1. Introduction

A review of current state-of-the-art femtosecond lasers with the currently record power of the order of 1 PW is presented. Based on an analysis of the advantages and drawbacks of parametric amplification in comparison with laser amplification in a neodymium glass and sapphire crystal, it is shown that the use of parametric amplifiers is a promising approach to overcoming a petawatt barrier. Other concepts concerning multipetawatt lasers, including those based on the unique properties of laser ceramics, are also discussed.

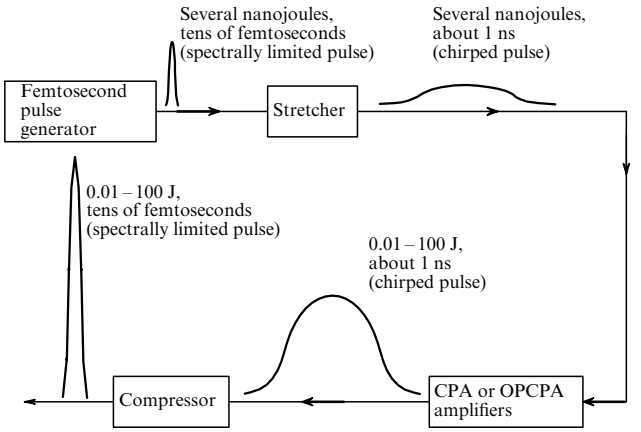

Figure 1. General drawing of powerful femtosecond lasers.

Since the creation of the first laser, one of the main goals of quantum electronics has been an increase in the peak power of laser radiation. The term 'high peak power' is continuously changing, and we are currently speaking of a power about 1 PW (10^{15} W). The key milestone that allowed obtaining such a power was the invention [1] of a fundamental principle, the amplification of chirped (stretched in time, frequency-modulated) pulses, CPA (chirped pulse amplification). The idea (see Fig. 1) is that prior to amplification, a femtosecond pulse is stretched to a duration of approximately 1 ns, which reduces its power and allows amplifying it to high energy without self-focusing and breakdown. Then the pulse is compressed to the initial duration using diffraction gratings with a high breakdown threshold, because light is only reflected from the gratings, not passing inside a material medium. The CPA principle is used without exception in all lasers with the power 1 TW or greater.

Petawatt power was first obtained in 1996 on the basis of CPA in neodymium glass [2]; the pulse duration was 440 fs and the energy was 600 J. The invention of sapphire crystal (corundum with titanium) [3] allowed obtaining considerably shorter pulses and resulted in the creation of a petawatt laser [4] with the much lower pulse energy of 28 J at the duration 33 fs. In Ref. [5], it was suggested to use the parametric amplification (optical parametric chirped pulse amplification, OPCPA) instead of the conventional laser amplification. The first petawatt OPCPA laser was created [6] in 2006 on the basis of a nonlinear DKDP crystal (Deuterated Potassium Dihydrogen Phosphate).

Thus, all existing petawatt lasers and those under development can be divided into three groups by the amplifying medium: (1) neodymium glass [2, 7–14], (2) sapphire (corundum with titanium) [4, 13, 15–17], and (3) parametric amplifiers on KDP (Potassium Dihydrogen Phosphate) and DKDP crystals [6, 18–25] (see Table 1). In all the groups, energy (in the form of population inversion) is stored in neodymium ions in a glass. In the first case, this energy is directly converted to the energy of a chirped pulse, which is then compressed. In the second and third cases, the stored energy is converted into the energy of a narrow-band nanosecond pulse, which is converted into a second harmonic and serves to pump the chirped pulse amplifiers. This pumping either provides the population inversion in a sapphire crystal or decays parametrically into two chirped pulses in a nonlinear crystal.